Supporting Information

Cost-Effective Nanocubic Prussian Blue Analogues for Enhanced Active-Barrier Epoxy Coatings

Xinyue Zhang, [a,c#] *Chunmei Zhang* [b*#] *Mairemu Maihaiti,* [a] *Kang Ye,* [a] *Xingzhi He,* [c] *Lingqian Ye,* [c] *Minjie Shi* [a,c*] *Jun Yang*[c], and *Edison Huixiang Ang*[d*]

[a] *School of Civil Engineering, Kashi University, Kashi 844000, P.R. China. E-mail: shiminjie@just.edu.cn*

[b] *School of Materials and Chemical Engineering, Henan University of Urban Construction, Pingdingshan 467036, P. R. China. E-mail: 942456323@qq.com*

[c] *School of Materials Science and Engineering, Jiangsu University of Science and Technology, Zhenjiang 212003, P. R. China.*

[d] *Natural Sciences and Science Education, National Institute of Education, Nanyang Technological University, Singapore 637616, Singapore. E-mail: edison.ang@nie.edu.sg*

Experimental section

Preparation of Mn-PBA

All analytical-grade chemicals were sourced from Aladdin Ltd. Potassium ferricyanide ($K_3Fe(CN)_6$) was addedto a mixed solution containing manganese acetate tetrahydrate ($Mn(CH_3COO)_2 \cdot 4H_2O$) and trisodium citrate dihydrate ($C_6H_5Na_3O_7 \cdot 2H_2O$) in a mass ratio of 33:70:55. The mixture was magnetically stirred for 5 min and subsequently was aged at room temperature for 36 h. The resulting precipitate was collected by centrifugation, washed several times with deionized water and ethanol, and finally was dried at 60 ℃.

Structural characterizations

To comprehensively evaluate the morphology and microstructure of the samples, the present study employed multiple characterization techniques, including field-emission scanning electron microscopy (FEI Nova NanoSem450, SEM), Fourier-transform infrared spectroscopy (Thermo Fisher Scientific Nicolet 6700, FTIR), X-ray diffraction (Bruker D8, XRD) equipped with a 2D detector (Cu Kα, λ = 1.54 Å), X-ray photoelectron spectroscopy (KAlpha Thermo electron, XPS), thermo gravimetric analysis (TGA5500, TGA) performed under an inert atmosphere, and electron paramagnetic resonance (EPR) spectroscopy (Bruker EMXplus-6/1, Germany).

Preparation of Mn-PBA/EP coating

An initial dispersion was prepared by ultrasonically dispersing Mn-PBA powder in ethanol. This suspension was uniformly blended with epoxy resin (EP) under continued ultrasonication, followed by heating at 40 ℃ to evaporate any residual ethanol. Subsequently, the curing agent was incorporated into the mixture at a mass ratio of EP

to curing agent of 5:4 under stirring. The final composite was deposited onto Q235 carbon steel by spin-coating using a homogenizer. After being oven-dried, the Mn-PBA/EP coating with a loading of 1% Mn-PBA was fabricated. Spin-coating was selected for this work because it enables the fabrication of coatings with uniform thickness, good surface homogeneity, and high reproducibility at the laboratory scale, thereby minimizing uncertainties arising from manual operation during performance evaluation. For comparison, Mn–PBA/EP coatings with Mn–PBA mass fractions of 0.5% and 2% were also prepared using the same method.

Anti-corrosion evaluations

The corrosion resistance of the coated samples was evaluated in a 3.5 wt% NaCl aqueous solution using a conventional three-electrode setup. The coated Q235 carbon steel served as the working electrode, with a platinum foil as the counter electrode and an Ag/AgCl electrode as the reference electrode. Electrochemical impedance spectroscopy (EIS) was conducted using a DongHua DH7003 multifunctional electrochemical workstation. Measurements were taken over a frequency range of 100 kHz to 0.01 Hz, applying a 20 mV sinusoidal potential perturbation during testing. Tafel polarization measurements were also performed to assess the corrosion rate of the coatings. Key electrochemical parameters, including corrosion current density (I_{corr}), corrosion potential (E_{corr}), and corrosion rate (V_{corr}), were derived from the Tafel extrapolation method. In addition, surface wettability was examined via water contact angle measurements using a contact angle meter (Attension Theta, Biolin Scientific)，

and pencil hardness was measured using a pencil hardness tester (QAQ, Jinan Chenxin Machinery Manufacturing Co., Ltd.).

To evaluate the water resistance of the Mn-PBA/EP, square specimens (1 cm × 1 cm, initial mass m_0) were immersed in 3.5 wt% NaCl solution for 240 h to simulate a marine corrosion environment. After immersion, the samples were rinsed with deionized water, thoroughly dried, and reweighed to obtain the final mass m_t. The water absorption Q_t was calculated using Equation S1:

$$Q_t = \frac{mt - m_0}{m_0} \times 100\% \quad \text{(S1)}$$

The resulting Q_t value after 240 h was only 2.6%, indicating excellent hydrophobicity and moisture barrier performance. This low water absorption is attributed to the hydrophobic characteristics imparted by the Mn-PBA within the EP matrix, which enhances cross-linking density and reduces surface energy, thereby effectively inhibiting water permeation. Such minimal absorption contributes to sustained coating integrity and enhances long-term anticorrosion performance by limiting electrolyte ingress and suppressing interfacial failure.

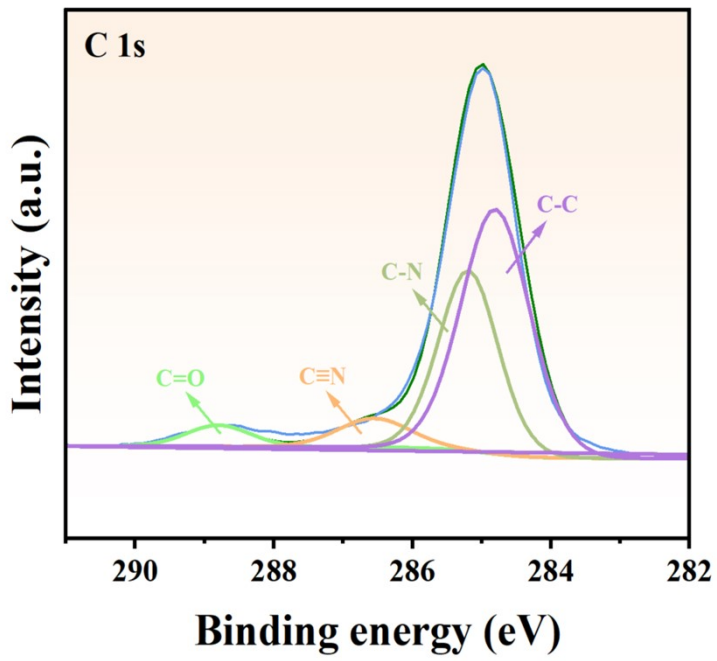

Figure S1. High-resolution XPS spectrum of the C 1s region for Mn-PBA.

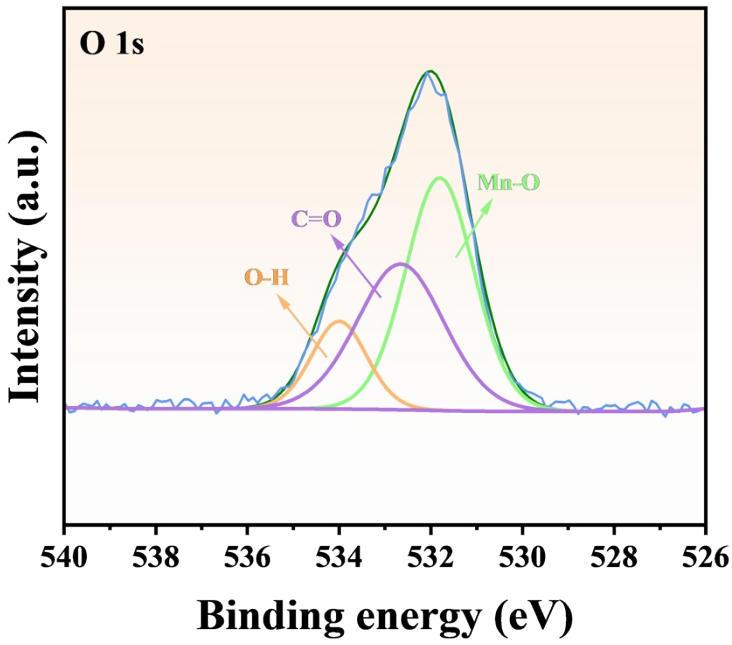

Figure S2. High-resolution XPS spectrum of the O 1s region for Mn-PBA.

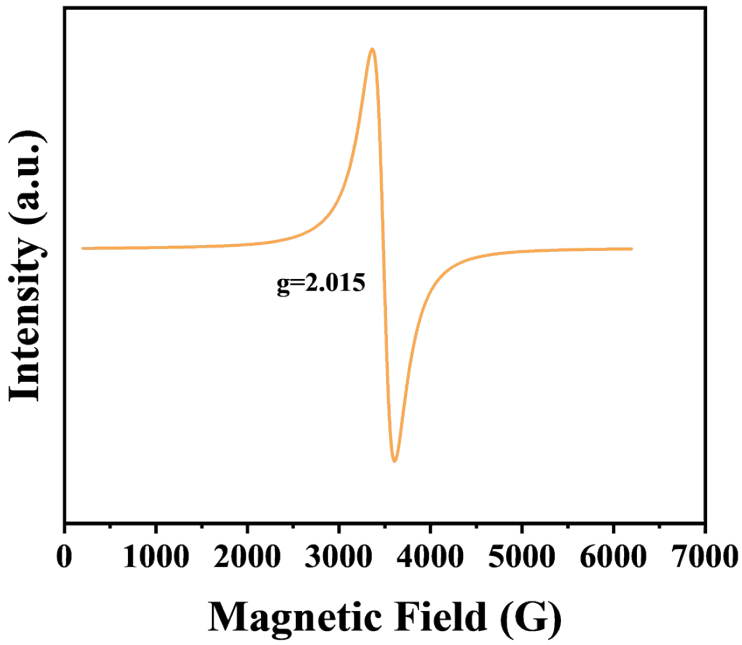

Figure S3. EPR spectrum of Mn-PBA.

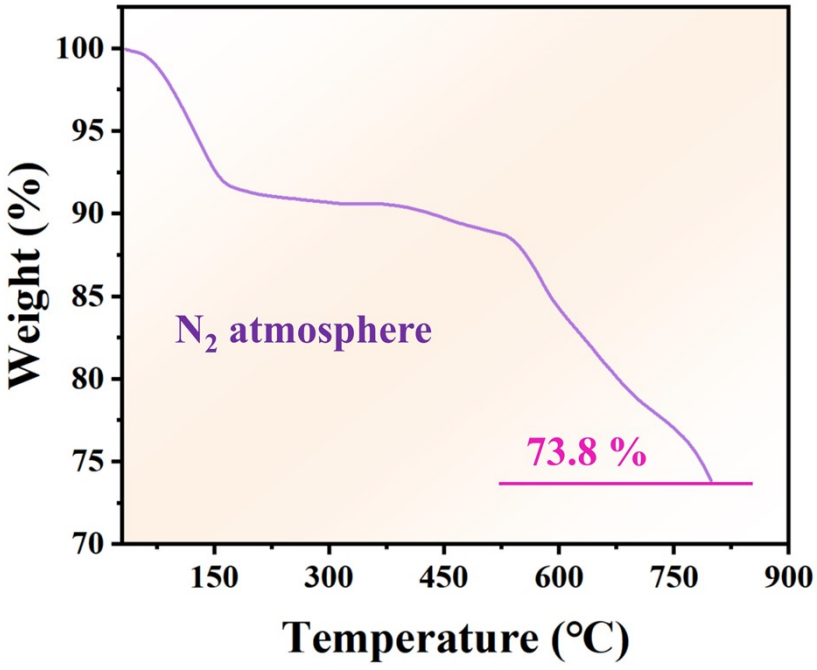

Figure S4. Thermogravimetric analysis (TGA) curve of Mn-PBA recorded under N_2 atmosphere, demonstrating its robust thermal stability.

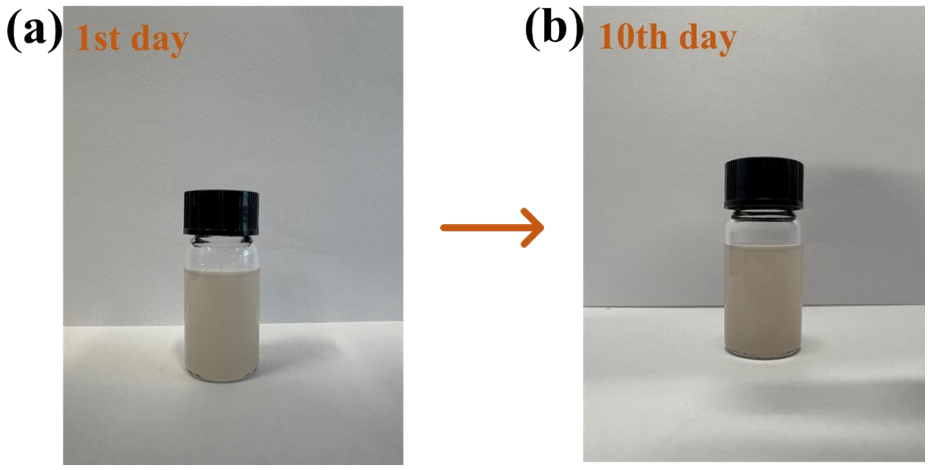

Figure S5. Comparison of Mn-PBA powder dispersion in ethanol: (a) Day 1 and (b) Day 10. The powder remains well-dispersed without noticeable sedimentation over the 10-day period.

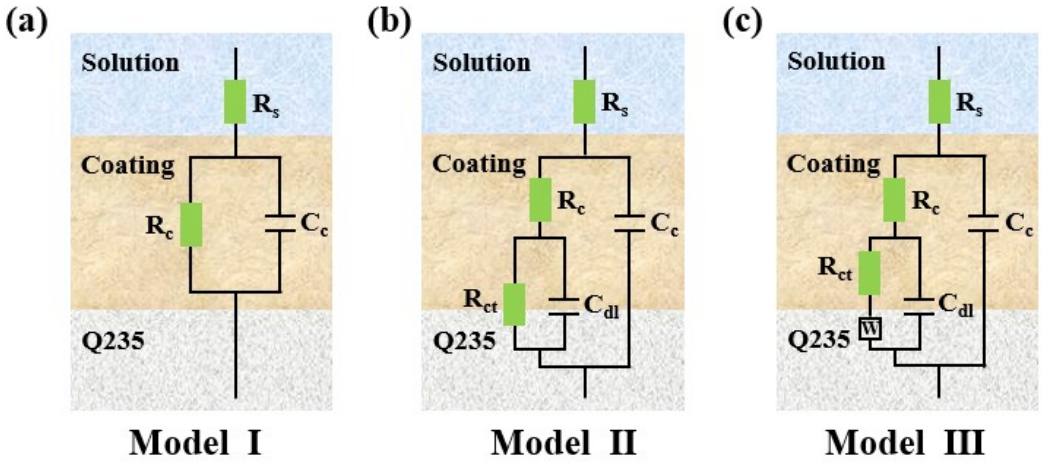

Figure S6. Equivalent circuit models used for fitting the EIS data.

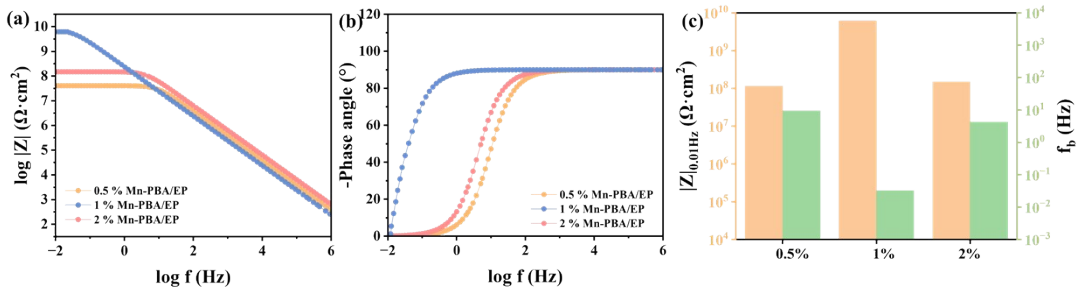

Figure S7. (a) Bode plots, (b) phase angle curves and (c) the corresponding $|Z|_{0.01Hz}$ and f_b values for Mn-PBA/EP coatings with varying filler contents (0.5%, 1%, and 2% by mass) in 3.5 wt% NaCl solution.

The electrochemical measurements indicate that the Mn–PBA/EP coating with 1% Mn–PBA exhibits the best corrosion protection performance among the investigated loadings, as reflected by its higher $|Z|_{0.01}$Hz, lower f_b, and overall improved anticorrosion behavior compared with the 0.5% and 2% samples (Fig. S7). At 0.5% Mn–PBA loading, the filler content is insufficient to effectively fill microvoids or establish a continuous tortuous barrier, thereby limiting both physical shielding and active protection; as a result, corrosive species can penetrate more readily, leading to inferior performance. At 2% loading, excessive filler induces particle aggregation and structural inhomogeneity, creating interfacial defects and reducing coating compactness, which compromises long-term protection. In contrast, the 1% Mn–PBA/EP coating achieves an optimal balance, where uniform filler dispersion produces a denser structure, an effective tortuous diffusion pathway, and an adequate density of redox-active sites for interfacial passivation.

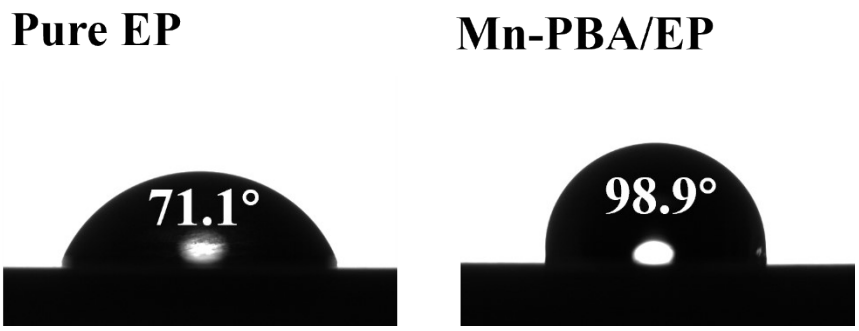

Figure S8. Contact angles of the pure EP and Mn-PBA/EP.

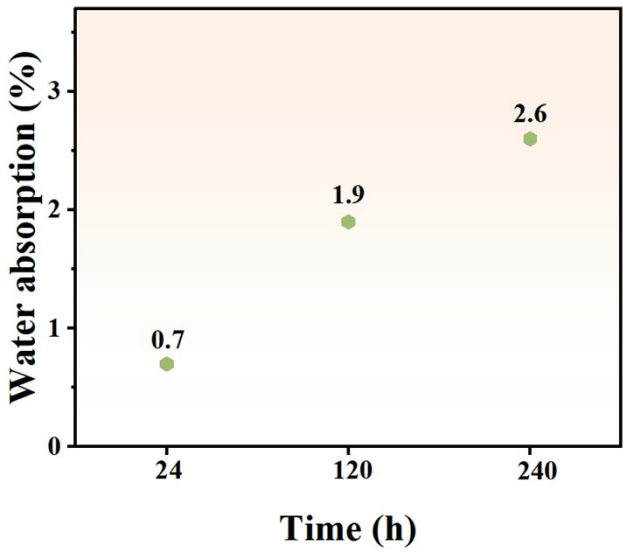

Figure S9. Water absorption of the Mn-PBA/EP coating as a function of immersion time.

As shown in Fig. S8, incorporating Mn–PBA increases the water contact angle of the coating from 71.1° for pure EP to 98.9° for Mn–PBA/EP, indicating a marked enhancement in hydrophobicity. Together with the reduced water absorption (Fig. S9), this suggests that Mn–PBA significantly improves the moisture-barrier capability of the epoxy coating, thereby helping to suppress the ingress of water and corrosive species. However, the improved anticorrosion performance of Mn–PBA/EP cannot be attributed solely to increased hydrophobicity. Given the open-framework structure and redox-active nature of Mn–PBA, an additional interfacial protection mechanism may also

contribute, particularly under prolonged immersion or locally damaged conditions where the purely physical barrier becomes partially compromised.

Therefore, the anticorrosion behavior of Mn–PBA/EP is more plausibly ascribed to a synergistic effect arising from enhanced barrier/hydrophobic properties and potential redox-assisted interfacial passivation.

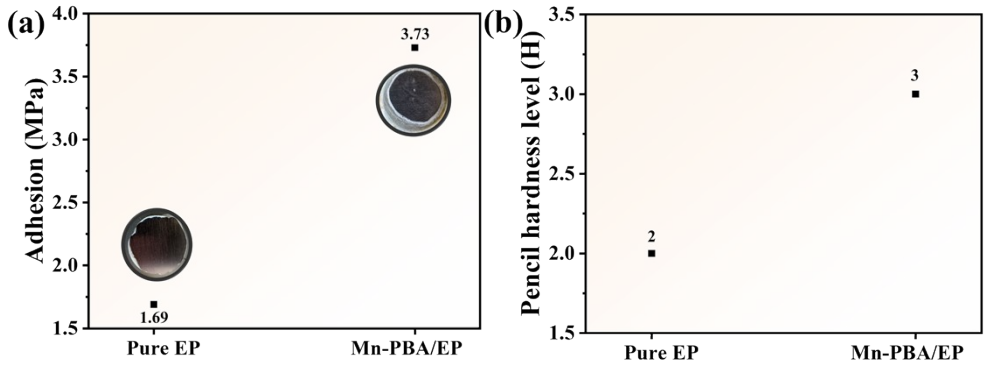

Figure S10. (a) Adhesion strengths and (b) pencil hardness level of pure EP and Mn-PBA/EP coatings.

Fig. S10a shows that the adhesion strength of the pure EP coating is only 1.69 MPa, whereas that of the Mn–PBA/EP coating increases markedly to 3.73 MPa, indicating significantly stronger interfacial bonding between the composite coating and the substrate. Meanwhile, the pencil hardness test results (Fig. S10b) reveal that the hardness of the pure EP coating is 2H, while that of the Mn–PBA/EP coating reaches 3H, demonstrating that the incorporation of Mn–PBA effectively enhances the coating's resistance to scratching and local deformation.

Carbon footprint

The carbon footprint shown in Fig. 1c was estimated using a simplified cradle-to-gate approach. The functional unit was defined as 1 ton of Mn–PBA product, and the results are expressed in t CO_2e per ton of product. The system boundary of this assessment includes the main processes involved in Mn–PBA production, namely raw material input, solution preparation, mixing, aging, separation, washing, and drying. The total carbon footprint was calculated by summing the contributions from material consumption and electricity use during the synthesis process. The activity data, calculation methodology, and emission factors used for each stage are summarized in Tables S1–S5. These tables provide detailed inventory data and parameter settings used in the estimation, thereby ensuring transparency and reproducibility of the carbon footprint analysis.

Table S1. Calculation methodology of carbon footprint.

Item	Description
Scope 1	Direct emissions from the process; assumed to be negligible because the aging step was carried out at room temperature without heating or combustion
Scope 2	Purchased electricity for stirring, aging control, centrifugation, drying, and deionized water preparation
Scope 3	Emissions associated with the production of raw materials and solvents, including $K_3Fe(CN)_6$, $Mn(CH_3COO)_2 \cdot 4H_2O$, trisodium citrate dihydrate, ethanol, and deionized water.

Table S2. Material inputs and corresponding emission factors (Scope 3).

Material	Consumption (kg/t product)	Emission factor (kg CO_2e/kg)	Carbon footprint (kg CO_2e/t product)
$K_3Fe(CN)_6$	7.31	4.2	30.70
$Mn(CH_3COO)_2 \cdot 4H_2O$	15.51	3.8	58.94
Trisodium citrate dihydrate	12.18	2.5	30.45
Ethanol	4.73	1.5	7.10
Deionized water	100	0.2	negligible
Scope 3 total			127.2

The unit material consumption was estimated from the precursor mass ratio 33:70:55 and the process recipe.

Table S3. Electricity consumption assumptions (Scope 2).

Unit operation	Assumption	Electricity use
Stirring	15 kW mixer; 5 min per batch; equivalent total time 2.38 h/t product	35.7 kWh
Aging	Room temperature, 36 h; only minimal control/monitoring power assumed (0.2 kW)	7.2 kWh
Centrifugation	30 kW centrifuge; total operating time 14.3 h/t product	429.0 kWh
Drying	60 °C industrial drying; estimated 100 kWh/t product	100.0 kWh
Deionized water preparation	RO electricity use≈2 kWh/m^3; 100 L water	0.2 kWh
Total electricity use		**572.0 kWh**

Using a grid electricity emission factor of 0.581 kg CO_2e/kWh, the Scope 2 carbon footprint was:

$$572.0 \times 0.581 = 332.3 \text{ kg } CO_2\text{e/t product}$$

Table S4. Total carbon footprint of Mn-PBA.

Category	Carbon footprint (kg CO_2e/t product)
Scope 1	0
Scope 2	332.3
Scope 3	127.2
Total	**459.5**

Thus, the estimated total carbon footprint is: 459.5 kg CO_2e/t product=0.4595 t CO_2e/t product

Table S5. Contribution of the main process stages.

Process stage	Carbon footprint (t CO_2e/t product)	Share (%)
Raw Material	0.1272	27.7
Aging Process	0.0249	5.4
Washing and drying	0.3074	66.9
Total	**0.4595**	**100**

Overall, the main carbon contribution arises from centrifugation, washing, and drying, while the contribution from raw material supply is secondary and that from aging is relatively small.